An Electrochemical and Photoelectron Spectroscopy Study of a Low Temperature Liquid Metal Battery Based on an Ionic Liquid Electrolyte

Lalau, C.-C.; Dimitrova, A.; Himmerlich, M.; Ispas, A.; Weier, T.; Krischok, S.; Bund, A.;

Originally published:

September 2016

Journal of the Electrochemical Society 163(2016)10, A2488-A2493

DOI: https://doi.org/10.1149/2.0051613jes

An electrochemical and photoelectron spectroscopy study of a low temperature liquid metal battery based on an ionic liquid electrolyte

Cornel-Constantin Lalau[a,z], Anna Dimitrova[b,z], Marcel Himmerlich[b], Adriana Ispas[a], Tom Weier[c], Stefan Krischok[b] and Andreas Bund[a]

[a] Electrochemistry and Electroplating Group, Ilmenau University of Technology, Gustav-Kirchhoff-Str. 6, 98693 Ilmenau, Germany

[b] Institute of Physics and Institute of Micro- and Nanotechnologies, Ilmenau University of Technology, PF 100565, 98684 Ilmenau, Germany

[c] Helmholtz-Zentrum Dresden-Rossendorf, Bautzner Landstr. 400, 01328 Dresden, Germany

[z] E-mail: cornel-constantin.lalau@tu-ilmenau.de

[z] E-mail: anna.dimitrova@tu-ilmenau.de

Abstract

We report the design of a low-temperature liquid metal battery (LMB). Li and Ga as the negative and positive electrode, respectively, are used in combination with a room temperature ionic liquid as an electrolyte. 1 mol/L lithium bis(**t**ri**f**luoromethyl**s**ulfonyl)**i**mide (Li[TFSI]) in 1-**b**utyl-1-**m**ethyl**p**yrrolidinium bis (**t**ri**f**luoromethyl**s**ulfonyl)**i**mide ([BMP][TFSI]) is chosen as electrolyte. The battery operates at 220 ˚C which is a relatively low temperature for a LMB and shows good electrochemical performance at low current density. The cells were cycled for more than 600 h and achieved a round-trip Coulombic efficiency close to 100 % and an average voltage efficiency of 66 % resulting in an overall energy efficiency of 65 %. At higher current densities, however, the system showed up to 75 % irreversible capacity loss after three cycles. To understand the origin of this strong deterioration, we characterized the surface and the bulk properties of the Ga cathode using X-ray Photoelectron Spectroscopy. Especially at higher

current densities a decomposition of the electrolyte was found. The occurring chemical changes and the elemental distribution at the Ga cathode are analyzed based on XPS measurements at different stages of the battery charge/discharge cycling.

1. Introduction

The rapid deployment of renewable energy technologies, such as solar and wind power, accelerates the need of new generation low-cost and long-life energy storage devices. To this end, various technologies have been proposed, such as hydroelectric pump storage, compressed air, fuel cells, flywheels and capacitors. However, they are often unable to provide satisfactory performance in terms of durability, high power, round trip energy efficiency and costs. Batteries are attractive as stationary storage devices due to their rapid response times, relatively high specific energy and energy densities (128 $Wh \cdot kg^{-1}$ and 230 $Wh \cdot L^{-1}$ for lithium-ion batteries, 150 $Wh \cdot kg^{-1}$ and 350 $Wh \cdot L^{-1}$ for sodium-sulfur batteries), high storage efficiencies and simple maintenance. However, their high cost and the safety risk prevent them from being widely adopted for stationary applications [1-4].

Recently the technology of liquid metal batteries (LMBs), first introduced in the early 60's, has been renewed [5-7]. The LMB tests in the Sadoway group at MIT provide valuable information about Mg/Sb, Li/Sb-Pb and Li/Bi systems and pointed out the promising features of these batteries such as their low production costs, their ability to work with high voltage efficiencies at high current densities when compared with conventional intercalation-type batteries and, last but not least, their ability to withstand a large number of charge/discharge cycles.

Typically, a LMB comprises three liquid layers, a low density alkali or earth alkali metal as negative electrode on the top, a high density molten metal as positive electrode at the bottom,

separated by a molten alkali halide mixture electrolyte with intermediate density [5]. The system self-stratifies due to density differences and immiscibility. During discharge, the molten metal at the anode is oxidized and cations are conducted through the electrolyte being reduced at the cathode and forming a liquid metal alloy. The process is reversed when the cell is charged. Depending on the selected electrode pairs and the used electrolytes, LMBs typically operate at high temperatures ranging from 450 to 700 °C. So far molten salt mixtures such as LiCl–LiBr, LiF–LiCl–LiI, are used as electrolytes in the LMBs [5-7]. In the present study we explore the suitability of **r**oom **t**emperature **i**onic **l**iquids (RTILs) as electrolytes in LMBs.

In recent years RTILs attracted a great attention due to their non-volatility, non-flammability, wide temperature range of operation and high conductivity [9,10]. They are already successfully used as electrolytes in rechargeable lithium batteries [11-13]. Those features of RTILs motivated us to explore their suitability as alternatives to molten salts for LMBs.

The advantage of operating at this relatively low temperature for such a system is the reduced reactivity of the molten electrodes with impact on the corrosion of the cell construction materials.

The electrolyte used in this study was a mixture of lithium bis(trifluoromethylsulfonyl)imide (Li[TFSI]) dissolved in 1-butyl-1-methylpyrrolidinium bis(trifluoromethylsulfonyl)imide ([BMP][TFSI]). The RTIL was chosen based on its good thermal and electrochemical stability and the low reactivity with molten lithium at the operating temperature (220 °C) [9]. In search of appropriate electrodes, we considered Li and Ga because of their low melting temperatures coupled with the binary phase diagram and the estimated equilibrium cell voltage [14]. Moreover, liquid Ga was already used as a self-healing negative electrode in lithium ion batteries and lithium shows good stability towards its halide melts and high discharge capacity [7, 8, 15].

2. Experimental

2.1. Electrochemical setup

Cells consisting of a Li negative electrode, a RTIL electrolyte mixture, 1 mol/L lithium bis(trifluoromethylsulfonyl)imide (Li[TFSI]) in 1-butyl-1-methylpyrrolidinium bis (trifluoromethylsulfonyl) imide ([BMP][TFSI]) and a Ga positive electrode were assembled in the fully charged state inside an insulating aluminum nitride ceramic tube with an active surface area of 0.68 cm^2 and then placed inside a cylindrical glass container (Fig. 1). Tungsten wires were used as negative and positive current collectors and the inter-electrode distance was 0.5 cm. The assembly process and the electrochemical characterization of the cells were conducted in an inert glove-box with argon atmosphere (OMNI-LAB from Vacuum-Atmospheres – O_2 content < 0.2 ppm, H_2O content < 0.5 ppm). The negative electrode was prepared by immersing the tungsten wire into the molten lithium. Then the gallium metal was added as liquid inside the AlN tube after which the RTIL electrolyte was poured and the negative electrode was placed on top of the electrolyte. The cells were heated up to 220 °C through a coil made of thermoresistive elements which was fixed around the glass tube. The temperature was measured and controlled with a thermocouple. The molten components self-segregate into three layers based on their immiscibility and density differences (0.512 $g \cdot cm^{-3}$ for Li, 1.4 $g \cdot cm^{-3}$ for [BMP][TFSI] and 6.095 $g \cdot cm^{-3}$ for Ga). Thus, based on the chosen geometry and the used materials, the assembled cells have a theoretical capacity of approximately 0.2 A·h.

According to the Ga-Li binary phase diagram, in order to maintain the all liquid metal alloy during operation at the chosen working temperature (220 °C) a fully discharged target composition of 7 mol. % Li in Ga was used [14].

Li and Ga were selected on the basis of their relative low melting points as compared to other existing electrode pairs (180.5 °C for Li and 29.7 °C for Ga). As precursors for battery assembly, Li (purity 99.9 %, supplier Alfa Aesar), Ga (99.99 %, Alfa Aesar), Li[TFSI] (99.9 %, Alfa Aesar) and [BMP][TFSI] (99.95 %, Iolitec) were used as received without further purification. The moisture content in the RTILs was monitored by Karl Fischer titration (model 831 KF from Metrohm) and an average value of 40 ppm water content was recorded.

Galvanostatic cycling with potential limitation (GCPL), cyclic voltammetry (CV) and electrochemical impedance spectroscopy (EIS) were employed to characterize the cells, using a two-electrode setup with Li metal serving as the counter/reference electrode and the Ga as the working electrode. The voltammetric curves were recorded between +1.1 V and +0.35 V at a scan rate of 0.5 $mV \cdot s^{-1}$ and the impedance spectra were acquired in the frequency range from 100 kHz to 10 mHz with an AC voltage amplitude of ± 10 mV around the open circuit potential. A Biologic potentiostat model SP300 was used for the electrochemical characterizations.

2.2. Sample preparation for XPS analyses

For analysis of the elemental distribution and the chemical composition of the Ga cathode's surface and bulk region, two Ga cathode samples (after discharge - lithiation and charge - delithiation, respectively) were carefully separated from the rest of the battery components prior to being packed into a hermetically sealed transfer-box for transportation. All the operations were done in a glove box under argon atmosphere.

117 2.3. XPS measurements and instrumentation

118 To prevent the samples from moisture/air exposure, a nitrogen dry-box (Carl Roth GmbH,
119 Germany) was mounted to the XPS spectrometer so that the samples could be easily removed
120 from the transfer-box within the dry-box, and placed into the transfer chamber.

121 XPS analysis were carried out with a Specs SAGE spectrometer (base pressure < 1×10^{-8} mbar)
122 equipped with a Phoibos 150 electron analyzer using a focused monochromatized AlKα radiation
123 ($h\nu$ = 1486.7 eV). During the experiments the pressure in the analysis chamber was ~ $5\times10^{-}$
124 ^{8} mbar. Core level spectra were recorded at a constant analyzer pass energy of 13 eV allowing a
125 total energy resolution of 0.6 eV and no charge neutralization was used. For binding energy
126 calibration, the energy scale was corrected by aligning the N1s signal to the N1s cation state of
127 the neat ionic liquid at 402.7 eV [BMP][TFSI] [16], while the binding energy (BE) scale of the
128 cathode sample was calibrated from the gallium signal using the $Ga2p_{3/2}$ peak at 1116.7 eV [17].
129 The core level spectra were analyzed by subtracting a Shirley-type background [18] and peak
130 areas were calculated by a weighed least-square fitting of model curves (70 % Gaussian, 30 %
131 Lorentzian) to the experimental data using the software package CASA XPS (Version 23.16
132 Dev52, Casa Software Ltd.). For quantification the atomic percentage (at. %) was calculated on
133 the basis of photoionization cross sections by Yeh and Lindau [8].

134 XPS sputter profiling was performed using a differentially pumped IQE 12/38 ion source
135 operated with Argon (source pressure 2.2×10^{-3} mbar, Ar^{+} ion energy keV, emission current
136 10 mA, ion current 6 mA) and laterally scanning the Ar^{+} ions across the sample surface (scan
137 area 10×10 mm^2). Under these conditions, the Ga-cathode can be etched at a rate of ~
138 0.2 nm·min^{-1}.

139

3. Results and discussion

3.1 Electrochemical performance

In order to investigate the electrochemical behavior of the Li||Ga LMB, several cells were assembled and tested at 220 °C. At this temperature, before the electrochemical test starts, the open-circuit potential (OCP) stabilizes at ~ 2 V, which strongly deviates from the reported thermodynamic data [20]. The deviation is probably caused by the formation of a passivation layer at the electrode-electrolyte interfaces as a result of interaction with the electrolyte. After several minutes of galvanostatic cycling, the OCP value stabilized at ~ 0.75 V. This change could correspond to a disintegration of the passivation layer during cycling.

The electrical conductivity of the RTIL electrolyte was estimated from the resistance at high frequency limit in EIS measurements and it was found to be 30 $mS \cdot cm^{-1}$, which is considerable lower than the conductivity of conventional molten halide salts typically used as electrolytes in LMB's (1.7–3.5 $S \cdot cm^{-1}$ for lithium halides).

The cell prototypes of ~ 0.2 A·h theoretical capacity were galvanostatically cycled at 10 $mA \cdot cm^{-2}$ (C/40 rate) for a predefined time of 20 h corresponding to a 50 % depth of discharge. The cut-off charging voltage was set to 1.11 V and the cells were operated continuously for about 600 h, i.e. for 14 charge-discharge cycles with stable cycling performance (Fig. 2). The near-constant voltage plateau observed in the galvanostatic voltage-capacity profile and the absence of a sharp voltage drop suggests that during the operation of the battery no intermetallic compounds are formed in agreement with the Li-Ga phase diagram. During the initial cycles the cells exhibited a round-trip Coulombic efficiency of 97 % which slowly increased to 100 % at the end of the test. This can be caused by an improved wetting of the tungsten negative current collector by molten

lithium during the cycling experiments. The cells achieved an average value of voltage efficiency of 66 % during the tests resulting in an overall energy efficiency of 65 %.

To gain further insight in kinetics of the LMB, we applied cyclic voltammetry (Fig. 3a) and electrochemical impedance spectroscopy (Fig. 3b). The charge-transfer overpotential, indicated by the deviation of the I=f (V) linear dependence in the CV experiment (Fig. 3a), is also confirmed by the presence of the depressed semicircle in the EIS scan (Fig. 3b). In the former the presence of more pronounced hysteresis in the anodic scan profile suggests irreversible phenomena during the charging (delithiation) process, which are further proved by XPS measurements (see Section 3.2).

The presence of the semicircle in the high frequency region can be attributed to the formation of a layer at the cathode-electrolyte interface, resulting from electrolyte decomposition products and can be defined as a **s**olid-**e**lectrolyte **i**nterface (SEI). Based on these findings one could estimate that the potential drop coupled with the charge-transfer overpotential plays an important role in the overall loss mechanism in the investigated system [21].

Our experimental results suggest that at low current densities and moderate time cycling a porous SEI layer is formed, facilitating the Li^+ diffusion into the cathode. This is confirmed by the slight decrease in the cell internal resistance observed in the figure 3b (EIS spectrum). At higher rates however, dense and impenetrable SEI structures might form, which hinder Li^+ diffusion out and into the cathode and lead to an increased capacity fade.

Further, in order to evaluate the battery capability, the cells were fully discharged (lithiated) at three different current rates: 10 $mA \cdot cm^{-2}$, 16 $mA \cdot cm^{-2}$ and 32 $mA \cdot cm^{-2}$, corresponding to a C/40, C/24 and a C/12 rate, respectively (Fig. 4). The cut-off voltage was set to 0.2 V for lithiation and

184 1.4 V for delithiation. At 10 $mA \cdot cm^{-2}$ the good electrochemical performance of the cells was
185 confirmed by a stable cycling behavior.
186 In the case of higher current rates (16 $mA \cdot cm^{-2}$ and 32 $mA \cdot cm^{-2}$) the batteries exhibit a
187 significant limitation in the delithiation process (see the capacity loss at Fig. 4), which suggest
188 irreversible phenomena occurring in the bulk of the electrolyte, at the SEI, or within the Ga
189 cathode.
190 In order to clarify the failure mechanisms within the battery, cells at different charge states were
191 slowly cooled down to room temperature and post mortem analyses were performed. When
192 opening the cell, it was visible that the RTIL electrolyte showed signs of degradation proved by a
193 change in color which turned to light-brown and also by the presence of fine particles
194 accumulated at the cathode-electrolyte interface. This might be caused by a SEI instability
195 coupled with RTIL decomposition products. Within the fracture cross-section of the cathode, a
196 distinct gray layer corresponding to the Li-Ga alloy, is present at the top, while liquid Ga is
197 observed beneath.
198
199 3.2 XPS analyses
200 As a next step we use XPS to determine the chemical composition on the surface and in the bulk
201 of two cathode samples. One was taken from a cell after the first complete lithiation, while the
202 other after a few electrochemical cycles, the last one being stopped at the end of the delithiation.
203 The BE positions of the surface detected core level states and the atomic concentration of the
204 elements are summarized in Table 1, and show a relatively good agreement between the
205 elemental composition and the peak positions of the neat [BMP][TFSI] ionic liquid [16] and the
206 Ga cathode surface. This refers to an electrolyte film, which does not evaporate after drying

under vacuum due to the very low vapour pressure of the ionic liquid. The increased amount of [TFSI] anion, suggested by the increased N^{anion}/N^{cation} (i.e, $N^{399.5\ eV}/N^{402.7\ eV}$) ratio, originates form the dissolved Li[TFSI] salt. No distinct presence of electrolyte decomposition products is found in this thin layer except a small amount of fluorine compound with BE = 685.3 eV ± 0.1 eV (0.8 at. % and 2.3 at. % after lithiation and delithiation, respectively), which we assign to LiF [22]. Its detection suggests electrochemical reduction of the [TFSI] anion to a reactive radical, $\bullet NSO_2CF_3^-$, which further breaks down to CF_2^- or F^--containing species, which easily react with metallic lithium and form RCF_2Li and LiF, as already proposed by Aurbach et al. [23] and Howlett et al. [24]. The absence of a Li^+ signal is assigned to the low photoelectron cross section of the Li1s state [19] and the related detection limit of XPS (0.1 at. %).

Further, we analyse the elemental compositions and the distribution in the bulk of the cathode after sputtering the samples with Ar^+ ions.

The BE positions and the quantitative analysis are displayed in Fig. 5 and Table 2. The detection of F, O, C, N and S inside the cathode is a direct indication for the decomposition of the electrolyte in the course of the electrochemical process and supports our assumption based on the EIS data. F, O, S and C – containing reduction products diffused irreversibly into the cathode layer already in the course of the first lithiation cycle and stay accumulated there after the liquid-solid transition during cooling of the battery system. S-containing species intercalate reversibly, while the N–containing reduction products are found only after a few cycles.

The deconvolution of the F1s spectrum reveals the presence of several species, which we assign to LiF (BE^{F1s} ~ 685.5 eV, BE^{Li1s} ~ 56 eV) [22] and three organic fluorine compounds detected at BE ~ 687, 689 and 691 eV. The peak at (~ 689 eV) has a position, which correlates with the

trifluoromethyl (-C$\underline{F}_3$) group from the $[TFSI]^-$ anion. The corresponding C1s peak however appears at BE ~ 289 eV, which is relatively low with respect to the $[TFSI]^-$ C1s peak of the neat ionic liquid (i.e. 293 eV) [16]. We assign this to an anion decomposition via cleavage of the F–C bond and formation of a $\underline{C}F^-$ containing $[TFSI]^-$ fragment (denoted as $R_1C\underline{F}^-$ in Fig. 5). Its further reduction leads to the formation of smaller species resulting in F1s state at ~ 687 eV. Finally, the fluorine component at ~ 691 eV points out to a subsequent rearrangement of the decomposition products and formation of species with $O–F_x$ fragment with a O1s peak at ~ 534.7 eV. Two additional oxygen states at ~ 533.2 and 531.2 eV indicate further incorporation of $\underline{O}$-C-$\underline{O}$ or C=$\underline{O}$ containing $[TFSI]^-$ reduction products (with corresponding C1s features at ~ 286-287 eV) and oxidation of Ga atoms, respectively. The $Ga2p_{3/2}$ state at ~ 1119 eV is characteristic for Ga–O bonds and the quantitative analysis of the corresponding components indicates formation of gallium oxyhydroxide (GaOOH) during lithiation and further transformation to gallium oxide (Ga_2O_3) during delithiation.

The C1s peak at ~ 285 eV has a characteristic BE for C-C/H bonds and most probably originates from the $[BMP]^+$ cation C_4H_9-alkyl chain. The detection of sulphur refers to $[TFSI]^-$ fragmentation, while the nitrogen signal might originate from both, the anion or the cation.

Next, we try to distinguish possible metallic and intermetallic states of Li and Ga. While the metallic Ga peak at 1116.7 eV is the most intensive one in the $Ga2p_{3/2}$ spectrum, there is no metallic Li detected in the bulk of the cathode (Fig. 5). The deconvolution of the Li1s spectrum identifies three components at ~ 56, 58 and 60 eV. As mentioned already, the first one originates from LiF, while the other two components at higher BE can only be explained by the presence of lithium–species, in which the $Li^{\delta+}$ positive charge is higher than that of LiF. This correlates well with two Ga-Li intermetallic states existing at room temperature: Ga_7Li_2 (BE = 58.0 eV) and

253 $Ga_{14}Li_3$ (BE 60 eV) [14]. The corresponding $Ga2p_{3/2}$ states are expected around 1120 eV, but are
254 not undoubtedly identified in the measurement. We anticipate that this is primarily connected to
255 an unexpectedly low amount of Ga detected after Ar^+ sputtering (Table 2), which might be due
256 to the sample roughness and the inhomogeneous distribution of the elements. Moreover, due to
257 the difference in kinetic energy the depth of information of the Ga2p photoelectrons is much
258 smaller than that of the Li1s photoelectrons.
259
260 **4. Conclusion**
261 A low temperature liquid metal battery with Li and Ga molten electrodes and an ionic liquid
262 based electrolyte (1M Li[TFSI] in [BMB][TFSI]) operated at 220 °C has been proposed and its
263 performances was evaluated. Low temperature LMBs are interesting candidates for fluid flow
264 measurements in multilayer systems. Cell prototypes of ca. 0.2 A·h theoretical capacity were
265 constructed and galvanostatically cycled at different current densities ranging from 10 $mA \cdot cm^{-2}$
266 (C/40 rate) to 32 $mA \cdot cm^{-2}$ (C/12 rate). The cells show promising performances at relatively low
267 current densities. The cells tested at 10 $mA \cdot cm^{-2}$ showed stable alloying and de-alloying with
268 discharge capacity values of about 100 mA·h at 50 % depth of discharge. Furthermore, the
269 round-trip Coulombic efficiency is close to 100 % with an overall energy efficiency of 65 %.
270 Further we checked the electrochemical behavior at higher current rates. At 16 $mA \cdot cm^{-2}$ and
271 32 $mA \cdot cm^{-2}$ the cells have almost identical performances, showing irreversible delithiation.
272 Increasing the current density rate induces a higher IR voltage drop coupled with charge transfer
273 losses contributing to a faster capacity fade. There are also indications of mass-transport
274 limitations of the Li ions at either of the electrode-electrolyte interfaces or within the electrolyte
275 or the Ga cathode. Our attempts to improve the battery performances by modifying the system

design did not succeed so far. However, in order to control the system, we tried to understand the processes which lead to the irreversible delithiation phenomena. X-ray Photoelectron Spectroscopy reveals that during the battery operation at 16 $mA \cdot cm^{-2}$, the ionic liquid based electrolyte decomposes already after the first discharge cycle and the reduction products accumulate in the Ga-cathode. Next to the metallic Ga in the bulk of the cathode, two Li-Ga intermetallic states are also detected: Ga_7Li_2 and $Ga_{14}Li_3$.

Acknowledgement

This work was supported by Helmholtz-Gemeinschaft Deutscher Forschungszentren (HGF) in frame of the Helmholtz Alliance LIMTECH. Additionally, we are thankful for research funding by the state of Thuringia and the European Union within the frame of the European Funds for Regional Development (EFRD) under grant 12021-715.

References

[1] G. L. Soloveichik, *Annu. Rev. Chem. Biomol. Eng*., **2**, 503 (2011).

[2] J. Kondoh, I. Ishii, H. Yamaguchi, A. Murata, K. Otani, K. Sakuta, N. Higuchi, S. Sekine, M. Kamimoto, *Energ. Convers. Manage.*, **41**, 1863 (2000).

[3] Z. Yang, J. Zhang, M.C.W. Kintner-Meyer, X. Lu, D. Choi, J.P. Lemmon, J. Liu, *Chem. Rev*., **111**, 3577 (2011).

[4] H. Chen, T. Ngoc Cong, W. Yang, C. Tan, Y. Li, Y. Ding, *Prog. Nat. Sci.*, **19**, 291 (2009).

[5] H. Kim, D.A. Boysen, J.M. Newhouse, B.L. Spatocco, B. Chung, P.J. Burke, D.J. Bradwell, K. Jiang, A.A. Tomaszowska, K. Wang, W. Wei, L.A. Ortiz, S.A. Barriga, S.M. Poizeau, D.R. Sadoway, *Chem. Rev*., **113**, 2075 (2013).

[6] D.J. Bradwell, H. Kim, A.H. Sirk, D.R. Sadoway, *J. Am. Chem. Soc.*, **134**, 1895 (2012).

[7] X. Ning, S. Phadke, B. Chung, H. Yin, P. Burke, D. R. Sadoway, *J. Power Sources*, **275**, 370 (2015).

[8] K. Wang, K. Jiang, B. Chung, T. Ouchi, P. J. Burke, D. A. Boysen, D. J. Bradwell, H. Kim, U. Muecke, D. R. Sadoway, *Nature*, **514**, 348 (2014) .

[9] H. Ohno, Electrochemical Aspects of Ionic Liquids, John Wiley and Sons, New York, 2005.

[10] A. Fernicola, B. Scrosati, H. Ohno, *Ionics*, **12**, 95 (2006).

[11] H. Sakaebe, H. Matsumoto, K. Tatsumi, *J. Power Sources*, **146**, 693 (2005).

[12] A. Ejigu, P. A. Greatorex-Davies, D. A. Walsh, *Electrochem. Commun.*, **54**, 55 (2015).

[13] S. Zhang, N. Sun, X. He, X. Lu, X. Zhang, *J. Phys. Chem. Ref. Data*, **35**, 1475 (2006).

[14] W.X. Yuan, W.J. Wang, Y.T. Song, X.L. Chen, *Scripta Mater.*, **48**, 1053 (2003).

[15] R. D. Deshpande, J. Li, Y. T. Cheng, M. W. Verbrugge, *J. Electrochem. Soc*., **158**, A845 (2011).

[16] S. Men, K.R.J. Lovelock, P. Licence, *Phys. Chem. Chem. Phys.*, **13**, 15244 (2011)

[17] J. F. Moulder, W. F. Stickle, P. E. Sobol, K. D. Bomben, Physical Electronics Division, Perkin-Elmer Corp, 1992.

[18] D. A. Shirley, *Phys. Rev*., **B 5**, 4709 (1972).

[19] J. J. Yeh and I. Lindau, Atomic subshell photoionization cross sections and asymmetry parameters: $1 \leq Z \leq 103$, At. Data Nucl. Data Tables, **32(1)**, 1 (1985).

[20] C. J. Wen and R. A. J. Huggins, *J. Electrochem. Soc*., **128**, 1636 (1981).

[21] M. E. Orazem and B. Tribollet, Electrochemical Impedance Spectroscopy, John Wiley and Sons, New York, 2008.

[22] L. Suo, Y.-S. Hu, H. Li, M. Armand, L. Chen, *Nat. Commun*., **4:1481** doi: 10.1038/ncomms2513 (2013).

[23] D. Aurbach, I. Weissman, A. Zaban, O. Chusid, *Electrochim. Acta***, 39,** 51 (1994).

[24] P. C. Howlett, N. Brack, A. F. Hollenkamp, M. Forsyth, D. R. Mac–Farlane, *J. Electrochem. Soc*., **153,** A595 (2006).

Table 1. Binding energy (BE in eV) and atomic percentage (at. %) of the elements F, O, N, C and S from XPS spectra of the neat IL alone and the cathode surface after lithiation (measured at the end of the first discharge cycle) and delithiation (measured after three cycles), corresponding to Figure 5.

	[BMP][TFSI]		Cathode surface after lithiation		Cathode surface after delithiation	
State	BE	at. %	BE	at. %	BE	at. %
F1s	689.0	25.7	688.9	28.3	688.9	22.8
			685.4	0.8	685.2	2.3
O1s	532.8	12.8	532.8	16.6	532.8	13.8
					531.2	1.4
N1s	402.7	2.6	402.7	2.8	402.7	2.3
	399.6	2.6	399.5	3.6	399.5	3.6
C1s	293.0	8.1	293.0	7.7	293.1	5.1
	286.8	21.6	286.8	13.6	286.7	11.6
	285.5	18.2	285.4	19.0	285.3	31.2
S2s	233.3	7.7	233.2	6.7	233.2	5.0
			230.2	0.9	229.5	0.8

Table 2. Binding energy (BE in eV) and atomic percentage (at. %) of the elements F, O, N, C, S, Li and Ga from XPS spectra of the Ga cathode after sputtering with 3 keV Ar^+ for 30 min (corresponding to Fig. 2)

	LITHIATION (30 min sputtering)		DELITHIATION (30 min sputtering)	
State	BE	at. %	BE	at. %
F1s	690.8	2.7	690.9	4.3
	688.9	3.5	689.2	3.1
	687.3	16.1	687.2	9.1
	685.6	6.3	685.7	2.7
O1s	534.5	4.0	534.9	2.7
	533.2	2.9	533.4	6.7
	531.2	1.5	531	1.8
N1s		—	391.9	5.4
		—	388.6	1.8
C1s	288.8	1.9	289	2.5
	287.4	7.0	287.3	11.1
	286.1	9.1	285.9	6.5
	285.1	10.6	285	11.3
S2s	234.4	1.5		—
	228.7	2.4		—
Li1s	59.9		60.6	
	58.0	28.0	58.0	29.5
	56.3		56.6	
Ga 2p	1120.4	0.5	1120	0.4
	1118.2	0.6	1118.3	0.6
	1116.7	1.3	1116.7	0.7
	1115.7	0.2	1115.9	0.1

Figure captions

Fig. 1 Schematic layout of the Li||Ga liquid metal battery.

Fig. 2 Electrochemical performance of a Li||Ga cell cycled at 10 $mA \cdot cm^{-2}$ for 50 % depth of discharge operated at 230 °C.

Fig. 3 Comparative cyclic voltammetric curves for a Li||Ga cell: initial (first – black and second – red voltammetric scans) and after 14 charge-discharge cycles at 10 $mA \cdot cm^{-2}$ (first – blue and second – magenta voltammetric scans). Scan rate: 0.5 $mV \cdot s^{-1}$ (a) and the Nyquist plots of a Li||Ga cell. Frequency range from 100 kHz to 10 mHz (b).

Fig. 4 Voltage profiles during charge-discharge cycles at different current densities of LMBs with theoretical capacity of 0.21 A·h.

Fig. 5 $Ga2p_{3/2}$, Li1s, C1s, F1s and O1s core level peaks XPS spectra of the bulk of the Ga cathode after lithiation (1) and after delithiation (2). The spectra are recorded after 30 min sputtering with Ar^{+}. The dashed spectra are the experimental ones, while the envelope peak is colored in blue and all fitted components are colored in black. The XPS spectra are presented in the order they are mentioned in the text.

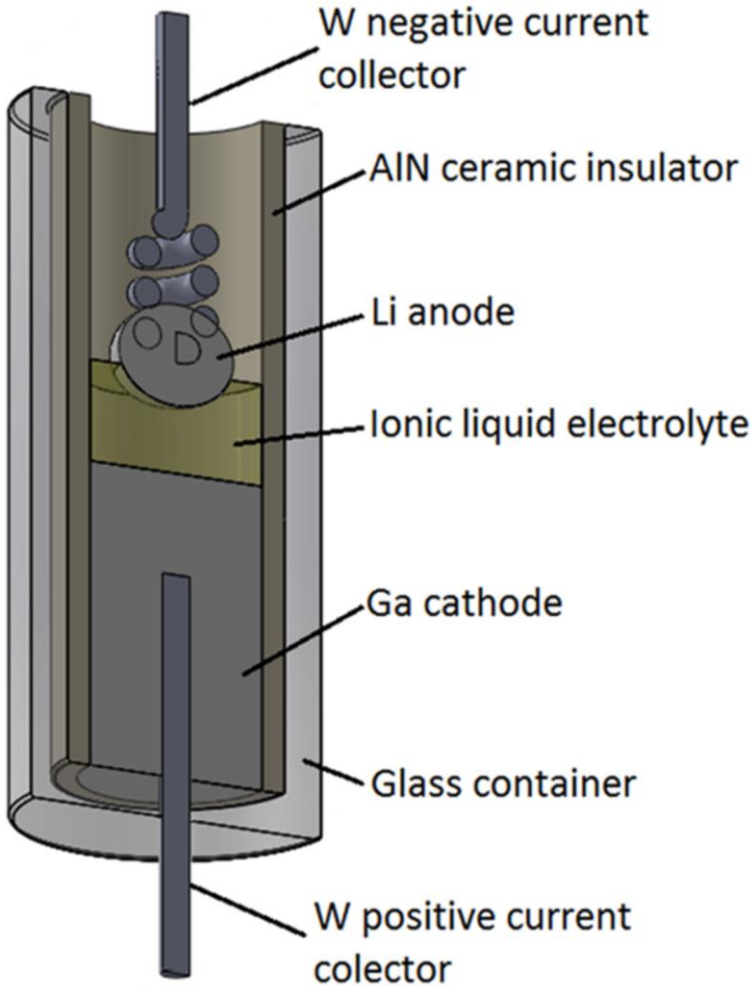
W negative current collector
AlN ceramic insulator
Li anode
Ionic liquid electrolyte
Ga cathode
Glass container
W positive current colector

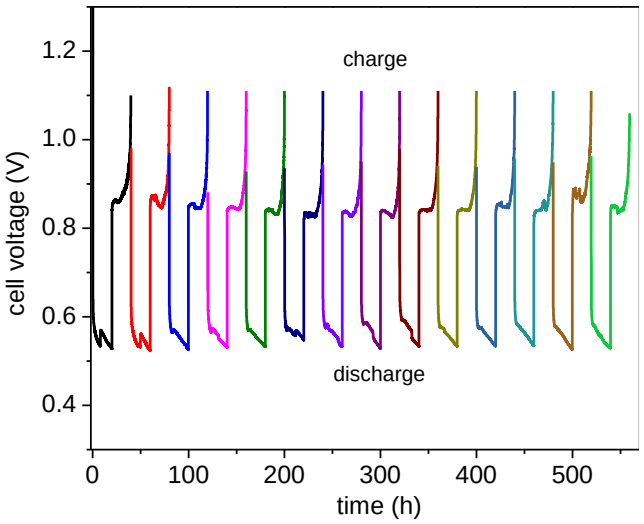
charge
discharge
cell voltage (V)
time (h)
1.2
1.0
0.8
0.6
0.4
0
100
200
300
400
500

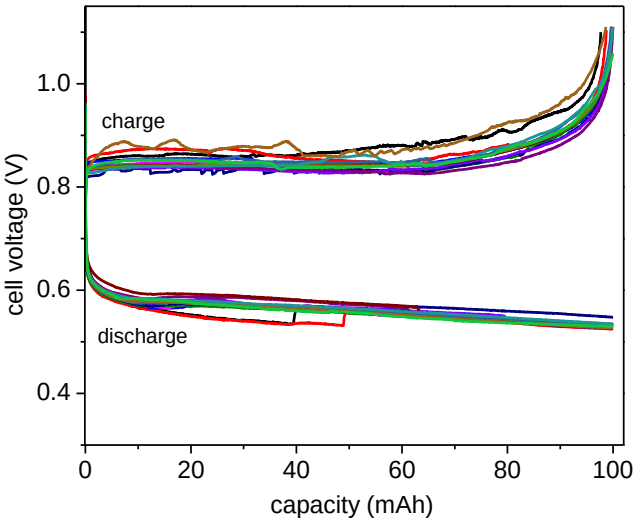
charge
discharge
cell voltage (V)
capacity (mAh)
1.0
0.8
0.6
0.4
0
20
40
60
80
100

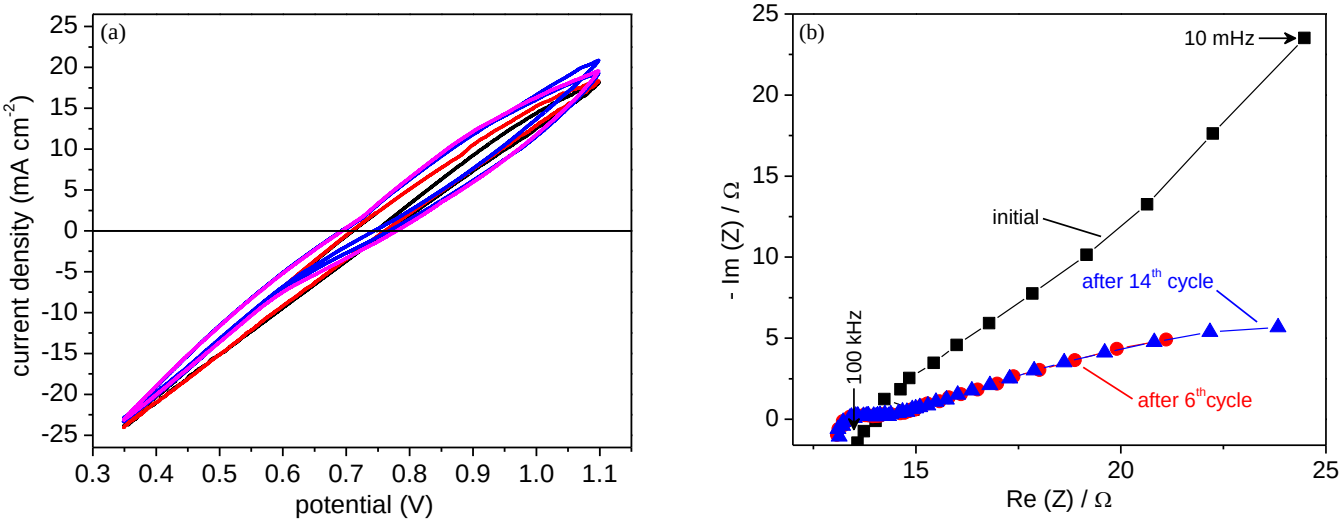
(a)
current density (mA cm-2)
potential (V)
25
20
15
10
5
0
-5
-10
-15
-20
-25
0.3
0.4
0.5
0.6
0.7
0.8
0.9
1.0
1.1
(b)
10 mHz
initial
after 14th cycle
after 6thcycle
100 kHz
- Im (Z) / Ω
Re (Z) / Ω
0
5
10
15
20
25

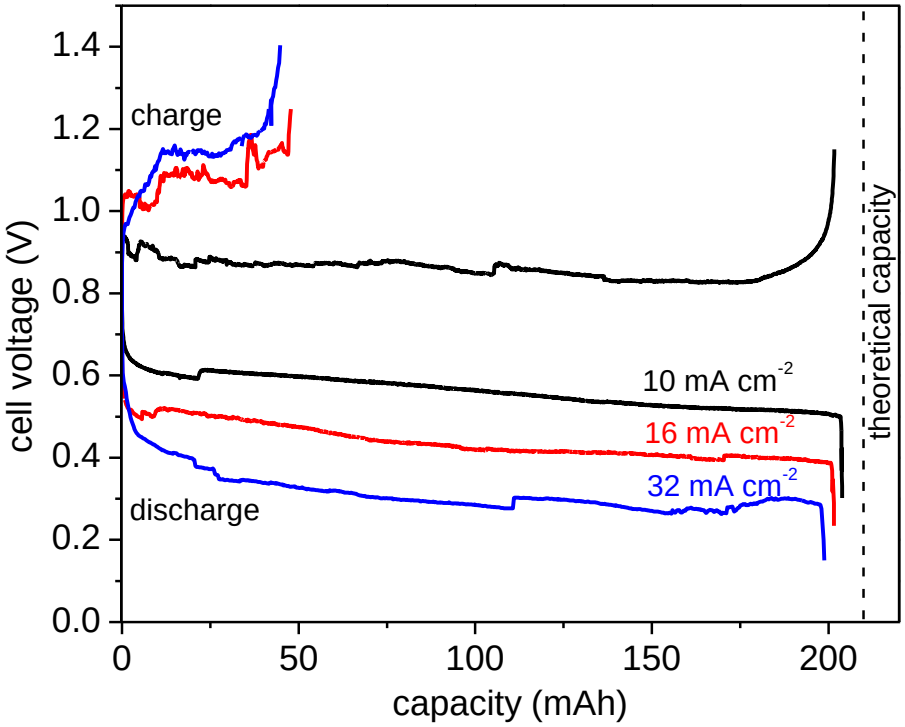
1.4
1.2
1.0
0.8
0.6
0.4
0.2
0.0
cell voltage (V)
0
50
100
150
200
capacity (mAh)
charge
discharge
10 mA cm-2
16 mA cm-2
32 mA cm-2
theoretical capacity

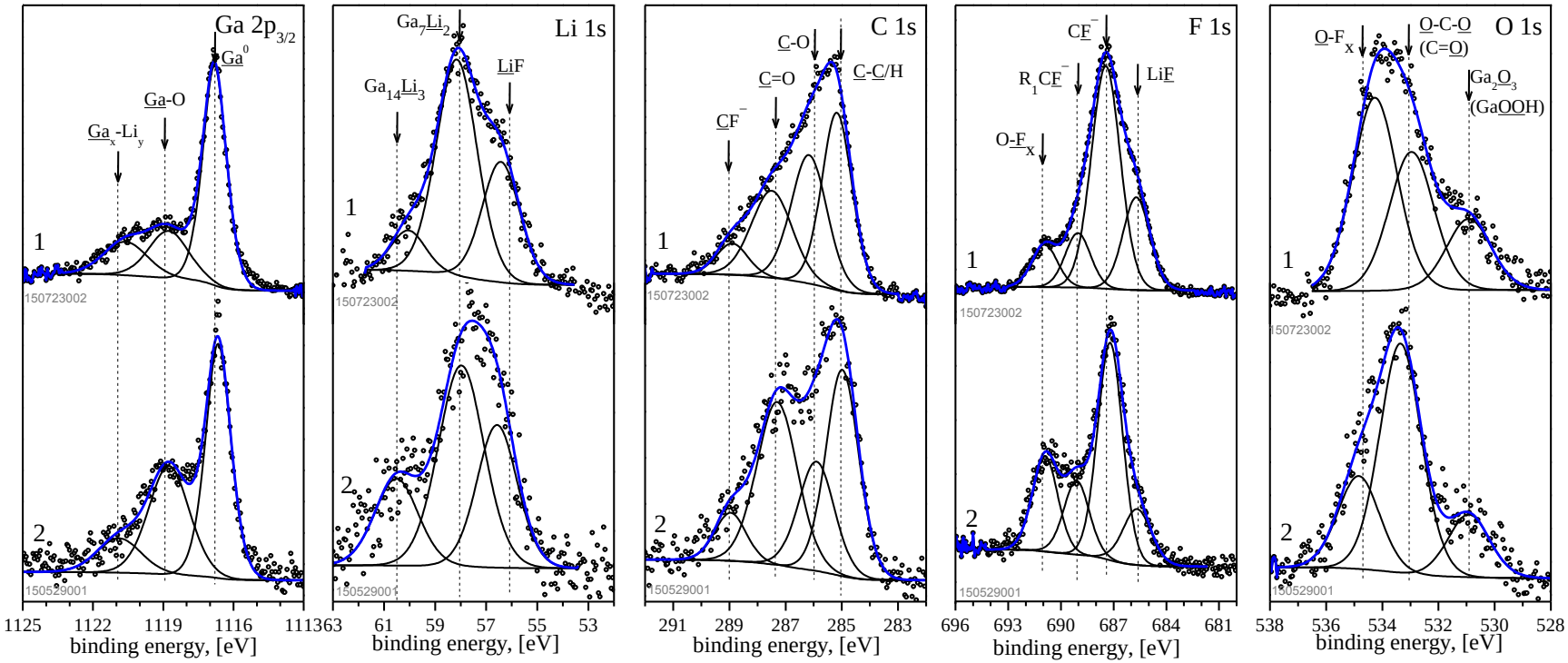
Ga 2p3/2
Ga0
Ga-O
Gax-Liy
1
2
150723002
150529001
1125
1122
1119
1116
1113
binding energy, [eV]
Li 1s
Ga7Li2
Ga14Li3
LiF
63
61
59
57
55
53
C 1s
C-O
C=O
C-C/H
CF−
291
289
287
285
283
F 1s
CF−
R1CF−
O-Fx
LiF
696
693
690
687
684
681
O 1s
O-Fx
O-C-O
(C=O)
Ga2O3
(GaOOH)
538
536
534
532
530
528